Supplement of Atmos. Chem. Phys., 21, 1613–1625, 2021
https://doi.org/10.5194/acp-21-1613-2021-supplement

Atmospheric Chemistry and Physics
Open Access

Supplement of

Low-NO atmospheric oxidation pathways in a polluted megacity

Mike J. Newland et al.

Correspondence to: Mike J. Newland (mike.newland@york.ac.uk) and Jacqueline F. Hamilton (jacqui.hamilton@york.ac.uk)

Contents

S1: Filtering data for mean diurnal plots – Figure 2

Diurnal plots of inorganic and organic species are shown in Figure 2 of the main manuscript for 'typical' chemistry days, i.e. where ozone increases through the morning to an afternoon peak of > 70 ppb. This accounts for 25 of the total 34 days for which ozone measurements are available. The days removed from the analysis were 22/5, 29/5, 2/6, 6/6, 8/6, 10/6, 22/6, 23/6, 24/6. Summer-time ozone in Beijing has been shown to be from both local production and regional transport of highly chemically processed regional air masses across the densely populated areas to the south of Beijing (Wang et al., 2017), with higher ozone episodes associated with a greater regional source (Streets et al., 2007). Beijing air quality is significantly influenced by air-masses that have passed over regions with large cities and inhabited by more than 500 million people (Parrish et al., 2016). The 'atypical', low-ozone days occur when the city is receiving cleaner air masses from the north of Beijing. The lower ozone leads to much higher concentrations of NO during the afternoon than on high ozone days. Figure S1 shows the diurnal profiles of NO, O_3, isoprene, ISOPONO2, and ISOPOOH+IEPOX for two atypical days (06/6, 10/6), compared to the mean diurnal cycle calculated from the 25 'typical' high ozone days. On 6 June, isoprene remains relatively low throughout the day, and there is no 'typical' morning NO peak, consequently, little ISOPONO2 or ISOPOOH+IEPOX are formed through the day. On 10 June, isoprene follows the mean campaign diurnal cycle closely, NO remains < 1 ppb throughout the afternoon, and peaks again in the evening, consequently the ISOPONO2 mixing ratio does not decrease through the late afternoon as for the mean campaign diurnal.

Figure S2 shows the ozone time series for the whole campaign. Figure S3 shows the mean diurnal variation of measured organic and inorganic species in the gas phase (as in Figure 2), with one standard deviation of the mean shown in the shaded areas. Figure S4 shows NO measurements for the whole campaign by hour for the afternoon hours of 12:00 to 20:00.

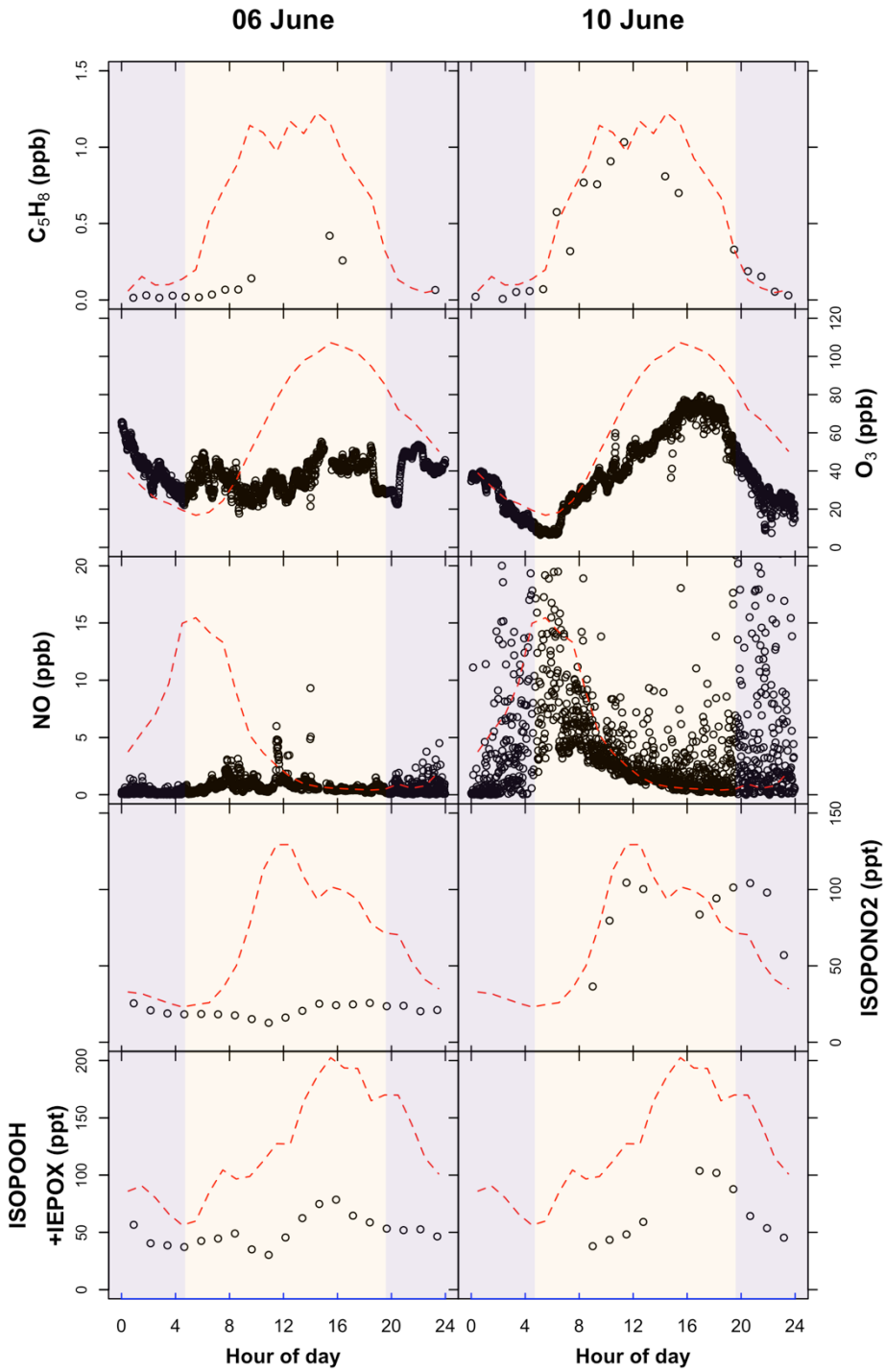

Figure S1 Comparison of mean diurnal cycle of isoprene, NO, O_3, ISOPONO2, and ISOPOOH+IEPOX during typical high ozone days with the atypical days 06 June and 10 June. The full time series have been filtered for days with afternoon ozone peaks < 70 ppb.

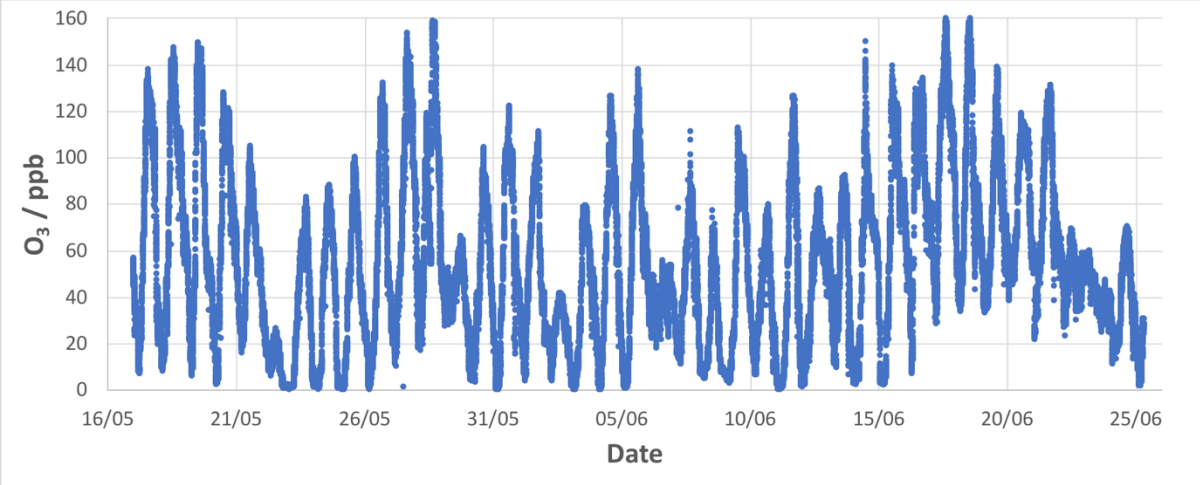

Figure S2 Ozone time series for the campaign. 17 May – 25 June.

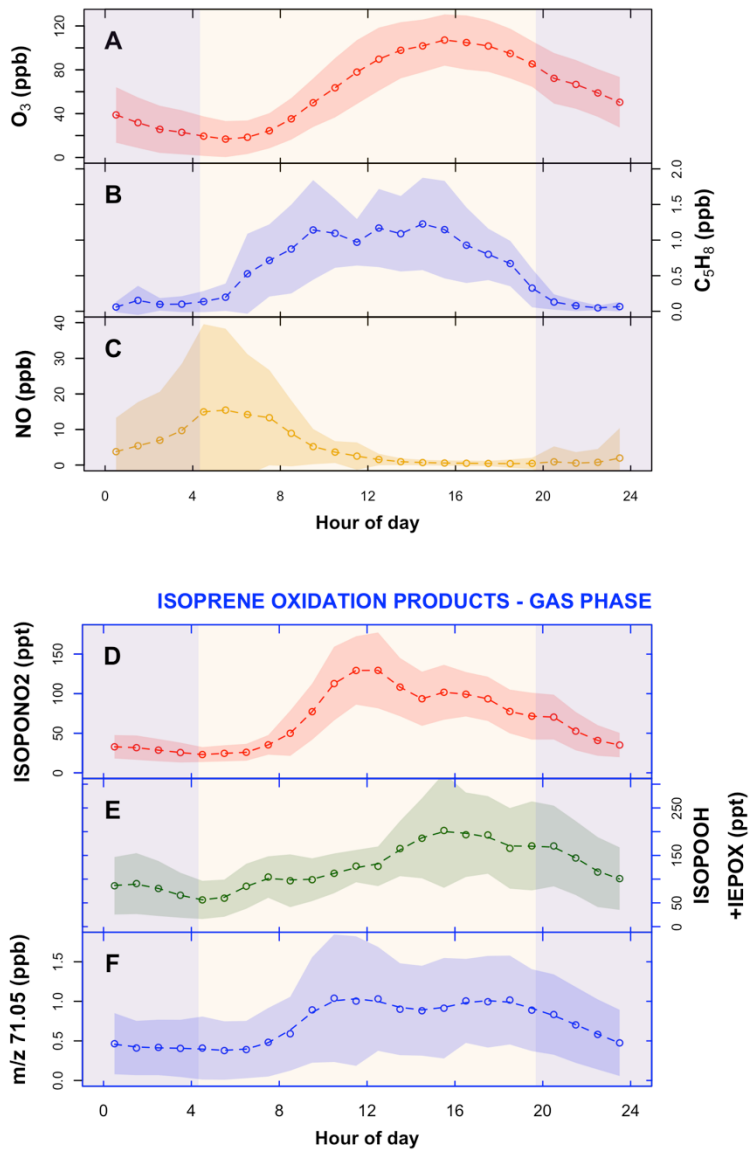

Figure S3 Mean diurnal variation of measured organic and inorganic species in the gas phase during the Beijing summer observations (as in Figure 2), with one standard deviation of the mean shown in shaded areas.

S2: Quantification of hourly [NO] decrease observed in the afternoon

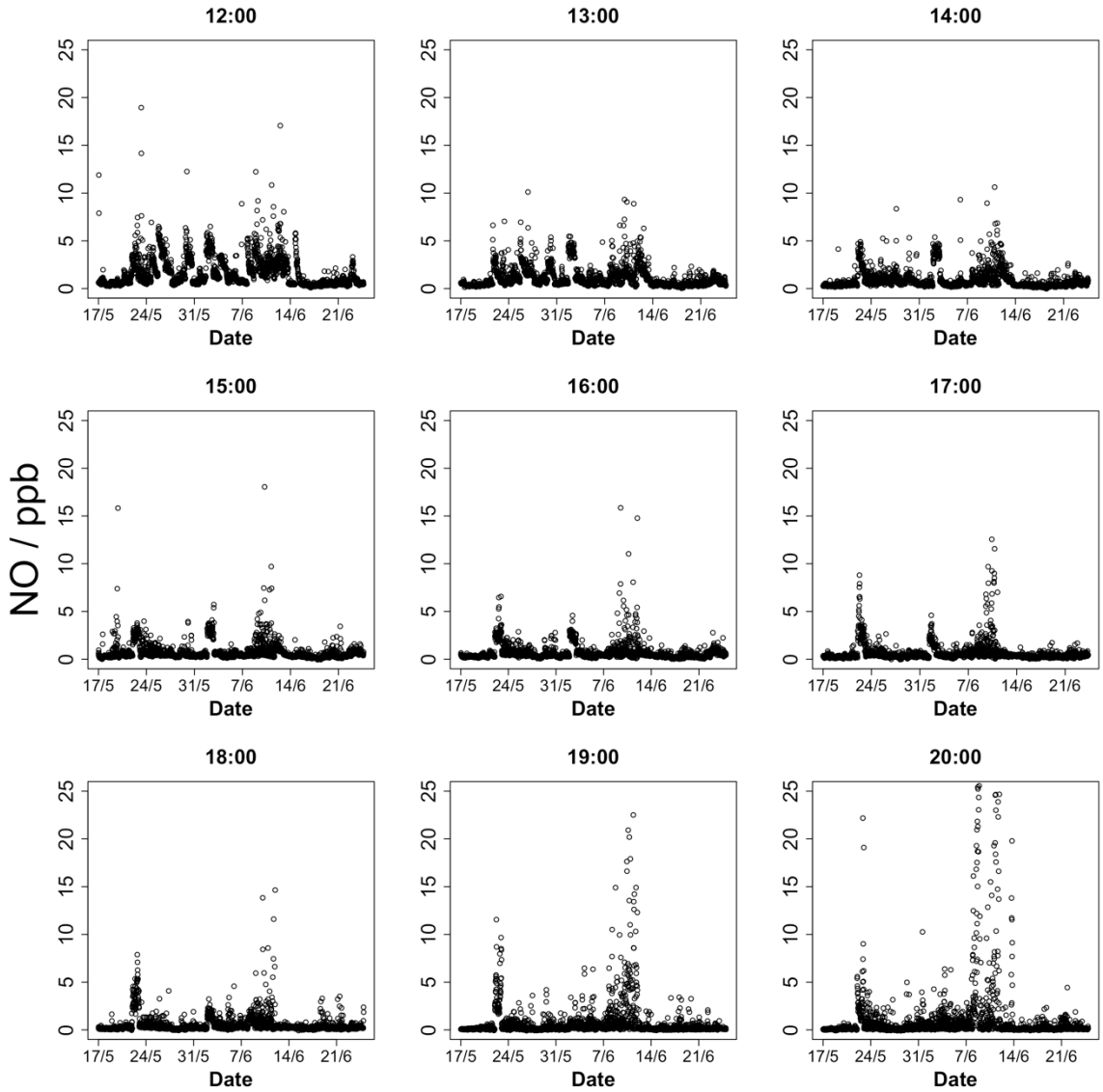

Figure S4 NO measurements for each hour between 12:00 and 20:00 for the duration of the campaign. Measurements at 1 minute frequency, i.e. 60 per day.

Figure S5 shows the mean hourly measurements of NO for each day of the campaign. A red dashed line between 12:00 and 20:00 represents the NO mixing ratio at which f_{NO} = 0.75, i.e. 25 % of ISOPOO is not reacting with NO, based on the mean hourly OH and OH reactivities for the whole campaign.

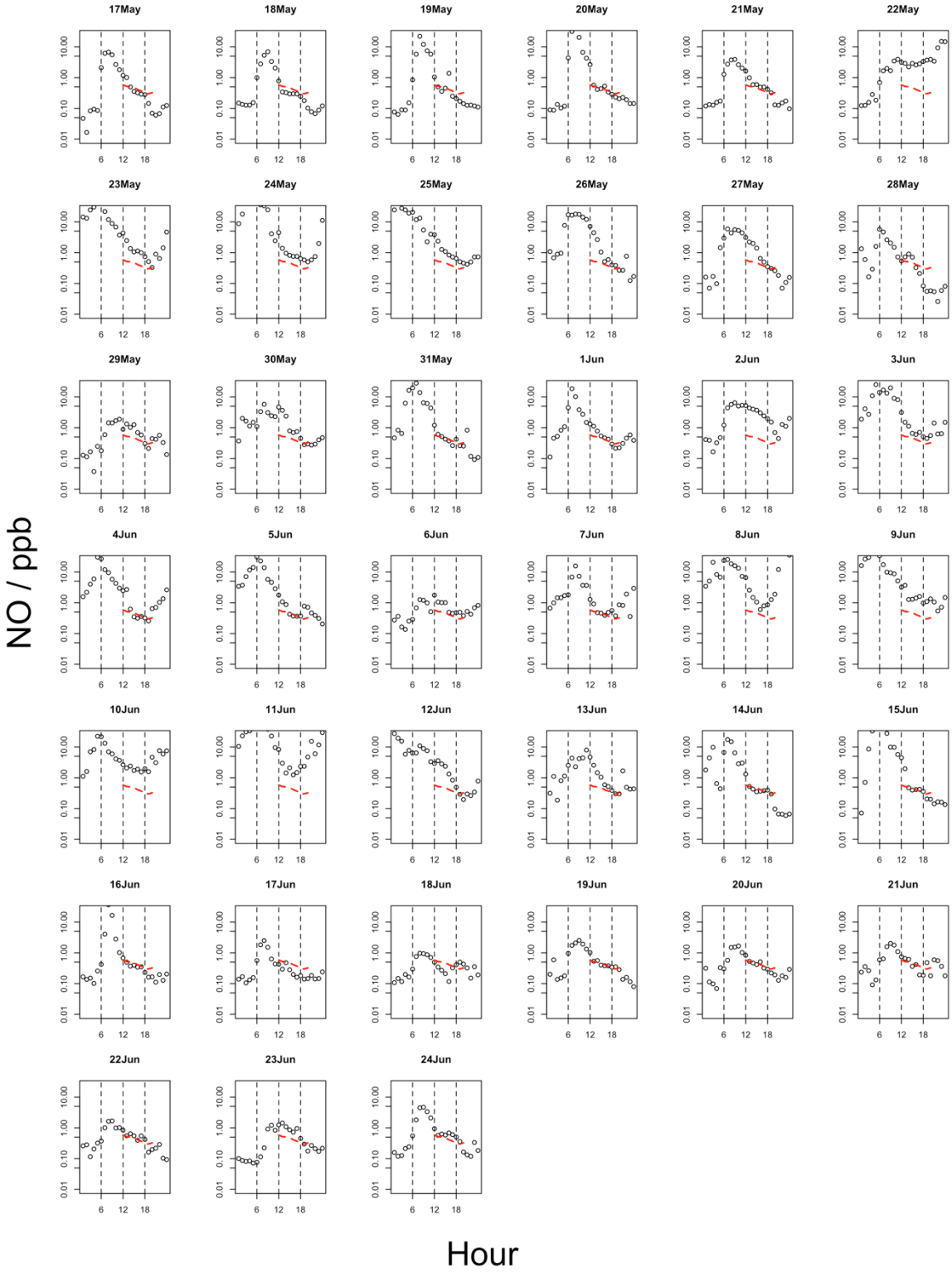

Figure S5 Mean hourly measured NO mixing ratios (ppb) during the campaign. Red dashed line between 12:00 and 20:00 represents the NO mixing ratio at which < 75 % of RO_2 are calculated to be reacting with NO.

S3: PTR-ToF-MS sampling details

The PTR-MS sampled air from three locations, as described in the Methods section. The data presented in Figure 2 is the 3 m data from the gradient sampling. Figure S6 demonstrates that there is very good agreement between the MVK+MACR signal measured in the air sampled from the flux inlet line sampling at 102 m as compared to the gradient sampling at 3 m and 102 m. The flux inlet line was made of PFA tubing and had an estimated 68 s transport time from the inlet to the PTR-MS at ground level, which then directly sampled the air in contrast to the sample being drawn into stainless steel containers for the gradient sampling.

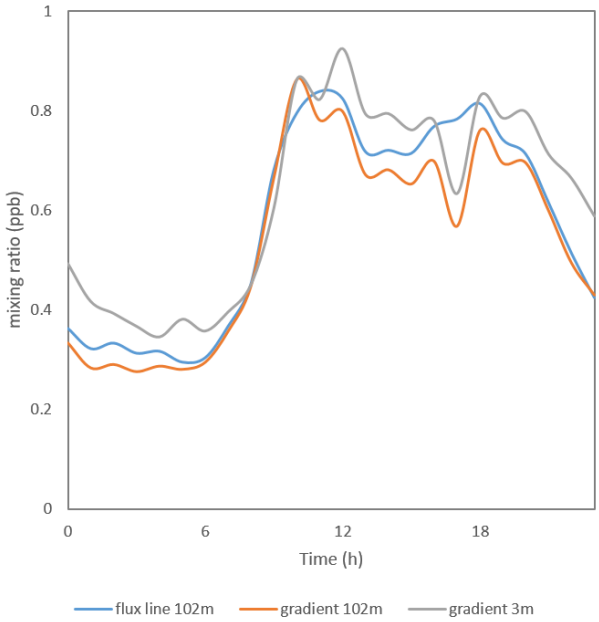

Figure S6 Mean diurnal MVK+MACR signal measured by the PTR-ToF-MS from two of the heights used for gradient sampling, and sampling from the flux inlet line.

S4: Figure 3 – Measurement data

Figure 3 in the main manuscript plots measured values of [OH] × OH reactivity* against [NO] between 12:00 and 20:00 for campaigns across a range of different environments. Only field campaigns where both OH and OH reactivity were measured can be plotted on Figure 3 (see Table S1) and the variability in NO levels in these regions is likely to be greater. For the Beijing dataset, the hourly median values of [NO] are used (Figure S7), with the 9 'atypical' chemistry days (as defined above) removed. Figure S6 shows the NO measurements for each hour between 12:00 and 20:00 for the whole campaign (excluding the 9 'atypical chemistry days) binned into 50 ppt bins between 0 and 1000 ppt. The median value takes into account all of the measurements including those above 1000 ppt not shown.

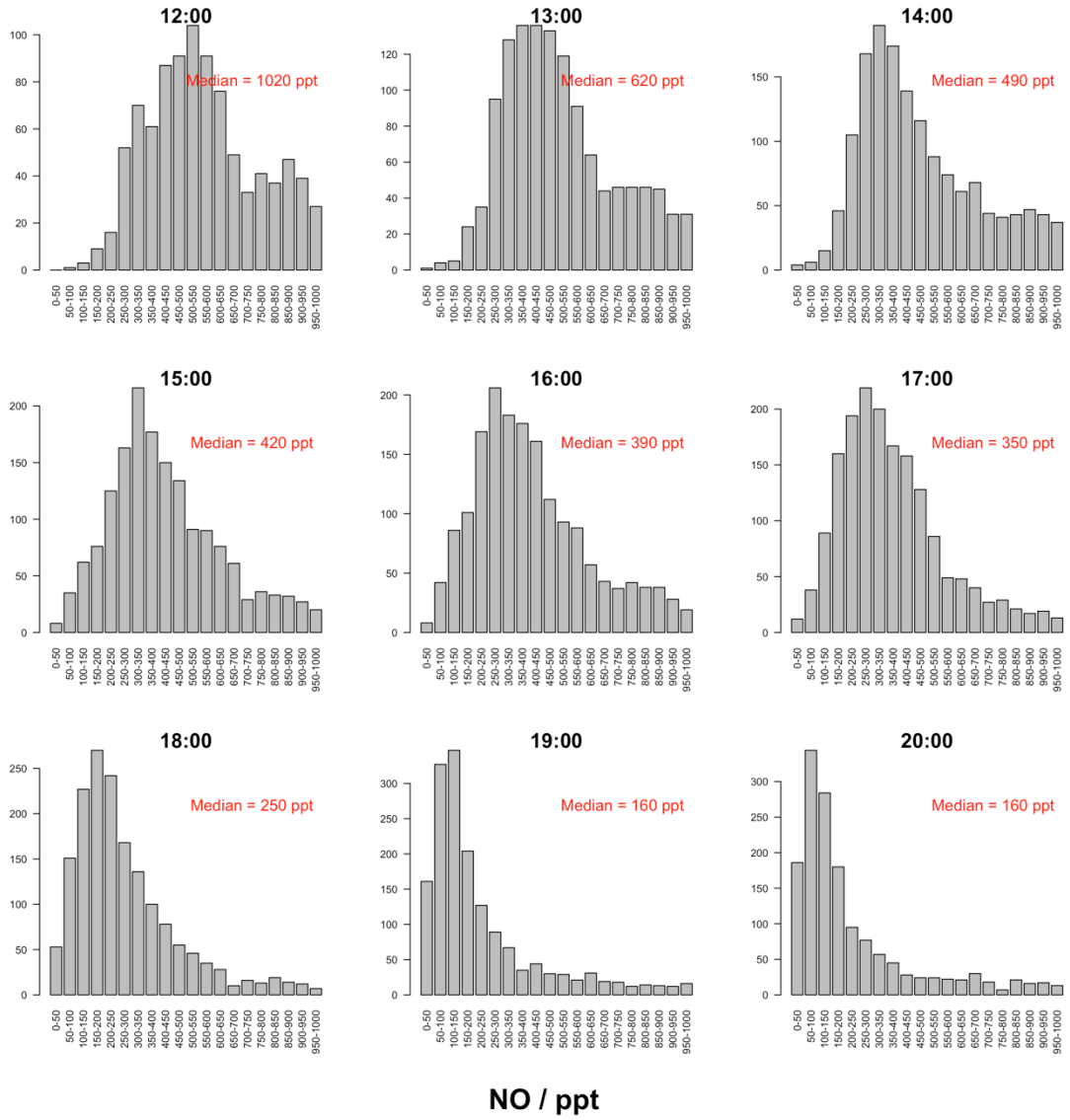

Figure S7 Distribution of minute averaged NO mixing ratios (ppt) during the campaign split in to 50 ppt bins for the hours 12:00 – 20:00, excluding the nine atypical days (see 'Filtering data for diurnals' above).

Table S1 details the location and measurement details of the NO, OH, and OH reactivity measurements presented in Figure 3 of the main manuscript.

Table S1 Details of measurement locations and conditions presented in Figure 3.

Location	Campaign	Date	HO_x and OH reactivity measurements Inlet position	Reference
NEW YORK Queens College, Borough of Queens (40° 44′ 15″ N, 73° 49′ 18″ W)	PMTACS - NY2001	June – August 2001	Co-located Scaffolding Tower at 6.4 m T = 279 – 308 K Average RH = 55 %	Ren et al. (2003)
BORNEO Burkit Atur GAW Station, Sabah Region (4° 58′ N, 117 ° 48″ E)	OP3 - I	April – May 2008	Co-located Container roof at 5 m T = 295 – 300 K	Whalley et al. (2011)
LONDON Sion Manning School, North Kensington (51° 31′ 61″ N, 0° 12′ 48″ W)	ClearfLo	July – August 2012	Co-located Container roof at 3.5 m T = 285 – 300 K	Whalley et al. (2016)
ALABAMA Centreville Research Site, Brent, SE – US (32° 54′ 11.81″ N, 87° 14″ 59.79″ W)	SOAS	June – July 2014	Co-located Tower at 15 m T = 301 – 303 K RH = 50 – 80 %	Sanchez et al. (2018)

S5: Box modelling

Table S2 Dry deposition velocities applied to all species based on their functional groups – based on Nguyen et al. (2015).

Functional group / species	Dry deposition velocity (cm s^{-1})
Hydroperoxide	2.0
H_2O_2	5.2
Organic nitrate	2.0
HNO_3	3.8
Organic acid	1.0
Oxygenated VOC	1.2
Other	0.1

Figure S8 shows the amount of ISOPOO reacting with NO ($\boldsymbol{f_{NO}}$), HO_2 ($\boldsymbol{f_{HO2}}$), RO_2 ($\boldsymbol{f_{RO2}}$), or isomerising ($\boldsymbol{f_{ISO}}$), for four different model runs with different fixed concentrations of C_5H_8 (i.e. OH reactivity) and OH. The point at which the contributions of the NO (f_{NO}) and HO_2 (f_{HO2}) channels are equal increases with increasing [OH] and with increasing OH reactivity, as shown in Figure 3 of the main manuscript. Figure S9 shows the modelled HO_2 and RO_2 concentrations for the same four model runs. As expected, both HO_2 and RO_2 increase with increasing [OH] and OH reactivity – this leads to the observed changes in $\boldsymbol{f_{NO}}$ and $\boldsymbol{f_{HO2}}$ in Figure S8. At very low [NO] (< 20 ppt), [RO_2] > [HO_2], although HO_2 dominates the reaction of ISOPOO because k(ISOPOO + HO_2) >> k(ISOPOO + RO_2) (Jenkin et al., 2015). As [NO] increases, [RO_2] falls rapidly, with [HO_2] falling less rapidly and becoming greater than RO_2.

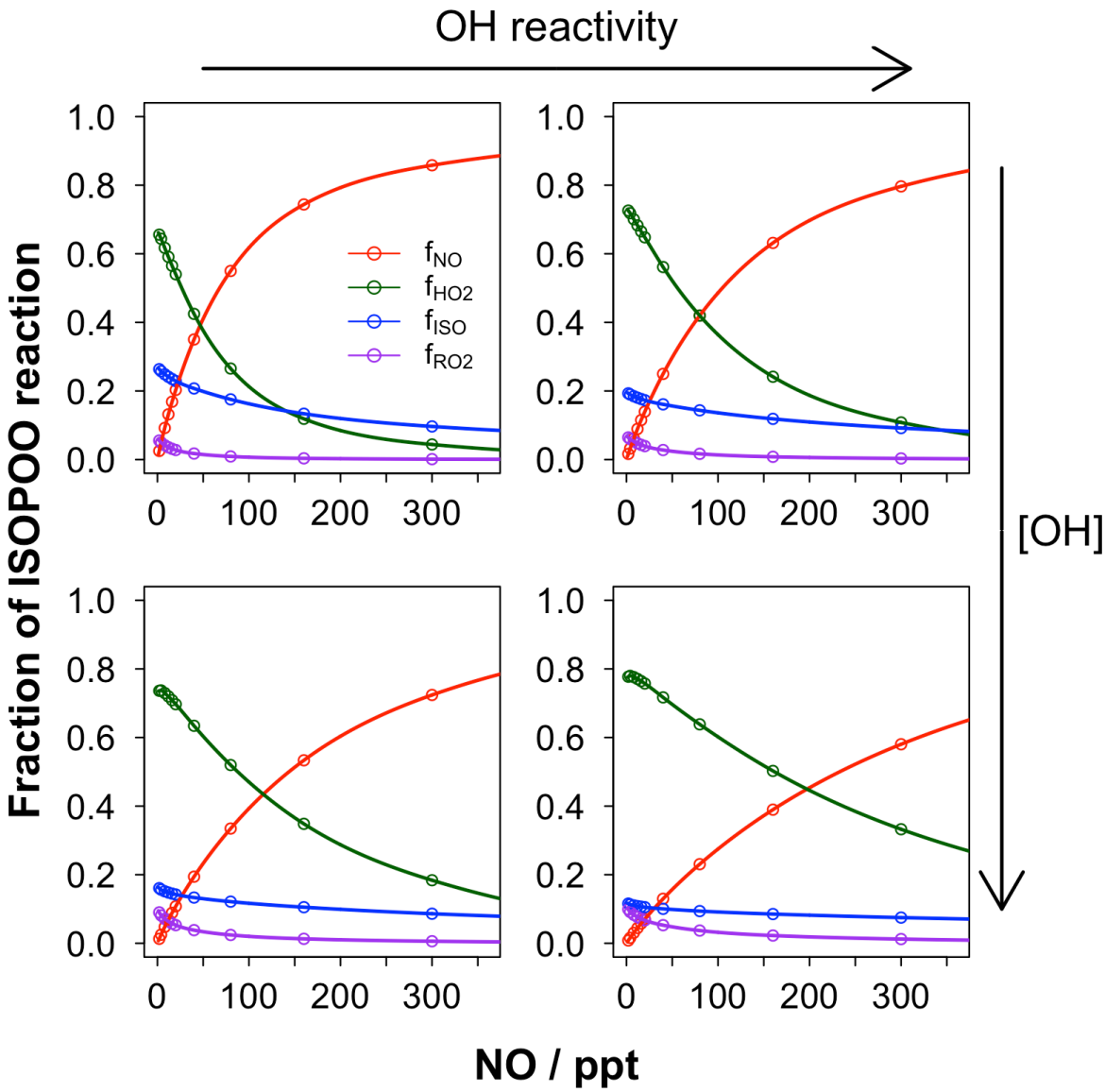

Figure S8 Example of model output showing the fraction of ISOPOO reacting with NO (f_{NO}), HO_2 (f_{HO2}), RO_2 (f_{RO2}), or isomerising (f_{ISO}), for four different model runs. Top left: $[C_5H_8]$ = 1.7 ppb, [OH] = 5×10^5 cm^{-3}; Top right: $[C_5H_8]$ = 5.0 ppb, [OH] = 5×10^5 cm^{-3}; Bottom left: $[C_5H_8]$ = 1.7 ppb, [OH] = 3×10^6 cm^{-3}; Bottom right: $[C_5H_8]$ = 5.0 ppb, [OH] = 3×10^6 cm^{-3}

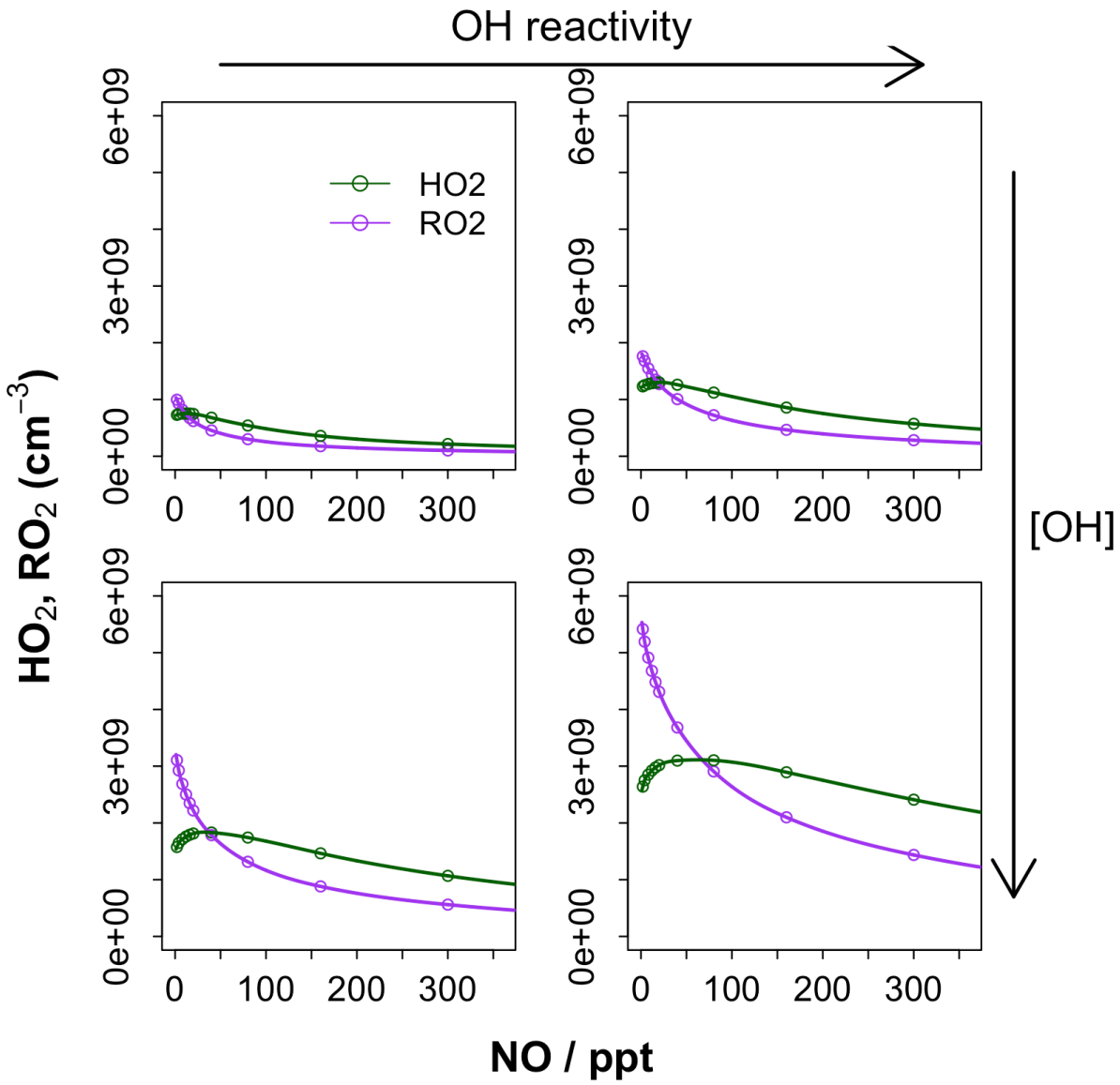

Figure S9 Example of model output showing modelled [HO_2] and [RO_2] for the four model runs shown in Figure S8. Top left: [C_5H_8] = 1.7 ppb, [OH] = 5×10^5 cm^{-3}; Top right: [C_5H_8] = 5.0 ppb, [OH] = 5×10^5 cm^{-3}; Bottom left: [C_5H_8] = 1.7 ppb, [OH] = 3×10^6 cm^{-3}; Bottom right: [C_5H_8] = 5.0 ppb, [OH] = 3×10^6 cm^{-3}

S6: Model calculated OH reactivity

The x-axis of Figure 3 in the main manuscript is OH x OH reactivity*, where OH reactivity* is defined as the OH reactivity attributable to VOCs (Equation E1) – i.e. without contributions from OH+NO_x (as this reaction does not make any RO_2 species). The total OH reactivity as a function of [NO] from an example model run, for which [C_5H_8] = 3.4 ppb and [OH] = 1 x 10^6 cm^{-3} is shown in Figure S10. The modelled OH reactivity is highest at low NO concentrations, with the main contributions from isoprene hydroperoxides (produced from ISOPOO+HO_2) and the parent VOC isoprene. At higher NO concentrations, the reactivity first decreases as production of isoprene hydroperoxides decreases, at even higher NO concentrations, OH reactivity begins to increase again as contributions from NO and NO_2 become important – however these do not contribute to OH reactivity*.

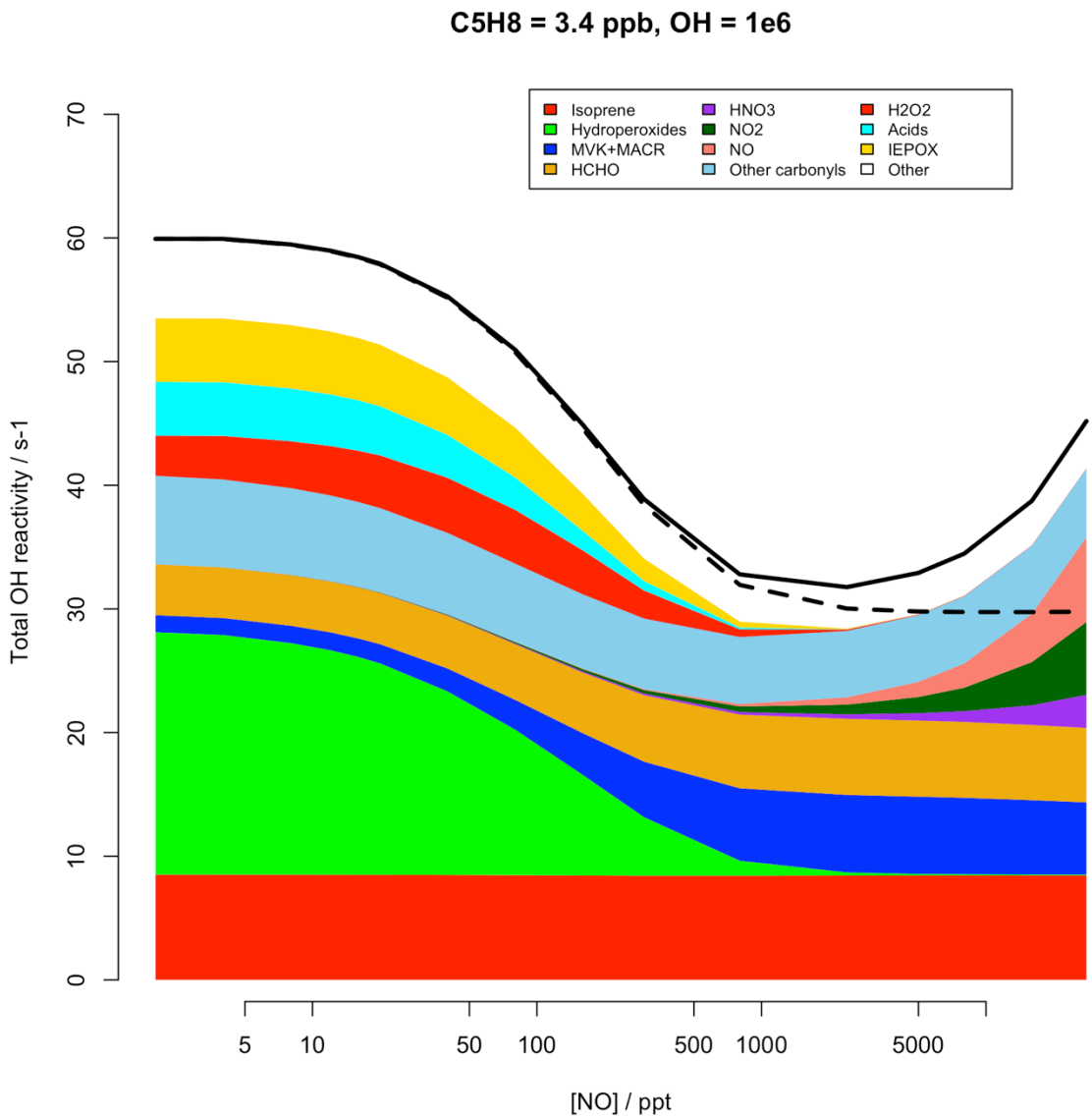

Figure S10 Modelled OH reactivity .v. [NO] for a model run initiated with $[C_5H_8]$ = 3.4 ppbv, [OH] = 1×10^6 cm^{-3}. Solid line is total OH reactivity. Dashed line is total OH reactivity*.

S7: Fraction of NO reacting with other RO_2

The box modelling for Figure 3 in the main manuscript is initialised with isoprene as the only VOC. Hence ISOPOO are the main (non-HO_2) RO_2 and the reactivity is dependent on isoprene and its oxidation products. However, the conclusions on the fate of ISOPOO drawn from the modelling hold for any other peroxy radicals, with minor variations. The fraction of RO_2 from a particular VOC that reacts with NO (i.e. f_{NO}) is dependent on the ratio of its reaction rate with NO (k_{NO}) to the sum of all the loss processes (Equation ES1).

$$f_{NO} = \frac{k_{NO}[NO]}{k_{NO}[NO] + k_{HO2}[HO2] + k_{RO2}[RO2] + k_{ISOM}} \qquad \text{(ES1)}$$

In the MCM, k_{NO+RO2} is the same value for the majority of RO_2, $2.7 \times 10^{-12}\ exp^{(360/TEMP)} = 9.0 \times 10^{-12}$ (298K) (with the exception of acyl-RO_2 for which it is 2.0×10^{-11} (298K) (Jenkin et al., 1997; 2019)). The other possible major sink for RO_2 under atmospheric conditions is reaction with HO_2. $k_{HO2+RO2}$ varies with carbon number in the MCM tending towards a maximum value of 2.3×10^{-11} (298K) (Jenkin et al., 1997)). Figure S11 shows the variation of f_{NO} as a function of [NO] for the initial RO_2 derived from isoprene, n-butane (a straight chain alkane), and toluene (an aromatic compound). f_{NO} follows the same trend for the RO_2 from all three VOCs. For both n-butane and toluene derived RO_2, f_{NO} is a little higher than for ISOPOO. For the example of straight chain alkanes, as the size of the alkane increases, f_{NO} would be expected to approach closer to the values for isoprene, as $k_{HO2+RO2}$ becomes faster while k_{NO+RO2} remains the same.

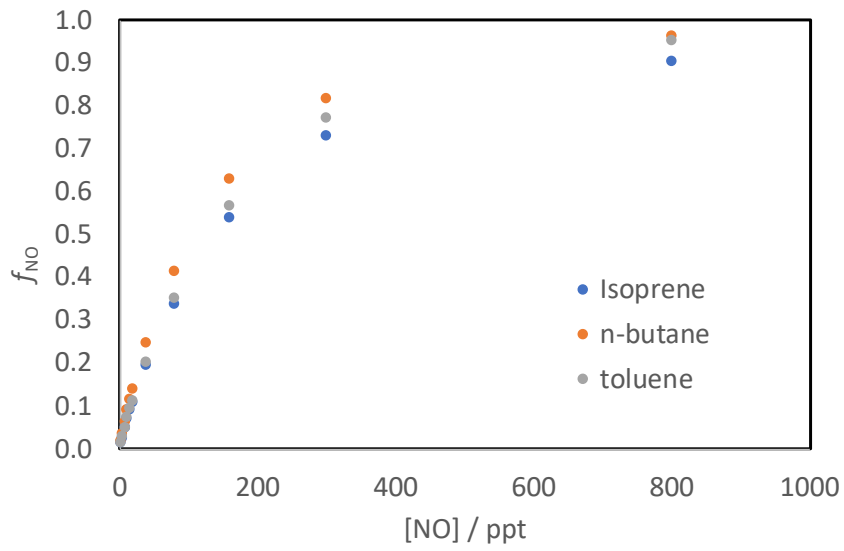

Figure S11 Variation of f_{NO} as a function of [NO] for the peroxy radicals formed in the initial OH-oxidation step of isoprene, n-butane and toluene.

References

Parrish D. D., Xu, J., Croes, B., and Shao, M.: Air quality improvement in Los Angeles – perspectives for developing cities, Front. Environ. Sci. Eng., 10, 2016.

Streets, D. G., Fu, J. S., Jang, C. J., Hao, J., He, K., Tang, X., Zhang, Y., Wang, Z., Li, Z., Zhang, Q., Wang, L., Wang, B., and Yu, C.: Air quality during the 2008 Beijing Olympic Games, Atmos. Environ., 41, 480-492, 2007.